Int. J. Heat Mass Transfer. Vol. 6, pp. 881–895. Pergamon Press 1963. Printed in Great Britain.

CONVECTION HEAT TRANSFER AND FLOW PHENOMENA OF ROTATING SPHERES

F. KREITH,* L. G. ROBERTS,† J. A. SULLIVAN‡ and S. N. SINHA§
University of Colorado, Boulder, Colorado

(*Received* 19 *September* 1962 *and in revised form* 28 *February* 1963)

Abstract—The flow engendered by and the convection heat transfer to or from a rotating sphere have been investigated experimentally and theoretically over ranges of Reynolds numbers from zero to 9×10^5, Grashof numbers from 7×10^4 to 3×10^9, and Prandtl numbers from 0·024 to 217. For Prandtl numbers between 4·0 and 217 and Reynolds numbers below 5×10^4 the average Nusselt number for cooling as well as heating was found to be in reasonably good agreement with the result of a theoretical analysis based on a solution of the boundary-layer equations in which the boundary-layer thickness around the sphere was assumed to be uniform. A detailed study of the boundary-layer flow by means of a hot wire and several visualization methods showed, however, that the thickness of the boundary layer increases with angular distance from the poles and that in the vicinity of the equator where the boundary layers from the upper and lower halves of a rotating sphere meet, a complex flow separation takes place. The extent of the separation region was determined and some unusual transition phenomena were observed.

NOMENCLATURE

a, radius of sphere;
A_s, surface area of sphere;
c, specific heat; c_p, specific heat of fluid at constant pressure; c_s, specific heat of solid sphere; c_v, specific heat of fluid at constant volume;
C, constant;
D, diameter of sphere;
g, gravitational constant;
h, average unit surface conductance of rotating sphere;
k, thermal conductivity;
K, δ_1/δ;
p, $(T_s - T_\infty)/2a^2\Omega^2$;
q, rate of heat transfer;
r, radial distance;
s, η/δ;
s_1, η/δ_1;
t, time;
T, temperature; T_∞, ambient fluid temperature;
u, radial velocity component;
v, tangential velocity component in a plane of a parallel;
w, tangential velocity component in a meridian plane.

Greek symbols

α, thermal diffusivity;
β, coefficient of expansion;
δ, hydrodynamic boundary-layer thickness;
δ_1, thermal boundary-layer thickness;
ϵ, emissivity;
η, dimensionless distance parameter $(\Omega/\nu)^{1/2}(r - a) = s\delta = s_1\delta_1$;
θ, acute angle subtended at the center of the sphere by any point and the nearest pole or latitude co-ordinate;
ϕ, meridian angle co-ordinate;
μ, absolute viscosity;
ν, kinematic viscosity;
ρ, density;
σ, Stefan–Boltzman radiation constant;
Ω, angular velocity;
Φ, extent of separation zone measured in degrees from equator.

* Professor of Mechanical Engineering and Chairman of the Superior Student Program.
† Research Assistant.
‡ Instructor of Mechanical Engineering, University of Michigan, Ann Arbor, Michigan, formerly Research Assistant, University of Colorado.
§ Assistant Professor, Bihar Institute of Technology, Sindri, India, formerly Graduate Student, University of Colorado.

Subscripts

c, convective;
f, fluid;
r, radiative;
s, sphere.

Dimensionless parameters

Gr, Grashof number, $g\beta(T_s - T_\infty)D_s^3/\nu_f$;
$\overline{Nu}$, average Nusselt number, $\bar{h}_c D_s/k_f$;
Pr, Prandtl number, $(c_p\mu/k)_f$;
Re, Reynolds number, $\Omega D_s^2/\nu_f$;
X, $\overline{Nu}/Re^{1/2}$.

INTRODUCTION

THE flow and convection heat-transfer characteristics of a sphere rotating about a diameter in an otherwise undisturbed medium are of interest in fluid mechanics, meterology, astrophysics and aeronautical engineering. The first study of such a system was undertaken by Sir George Stokes in 1845. Although Stokes was mainly concerned with the pressure distribution around a rotating sphere, he also gave a quite accurate description of the flow mechanism: "The sphere acts like a centrifugal fan, the motion at a distance from the sphere consisting of a flow outwards from the equator and inwards towards the poles, superimposed on a motion of rotation" [1].

It was not until more than a century later that the problem received again serious attention. Using boundary-layer approximations the flow engendered by a rotating sphere has recently been investigated theoretically by Howarth [2] and Nigam [3], and the temperature field in the vicinity of a heated sphere has been studied by Singh [4] in the laminar flow regime. Experimental measurements of velocity profiles have been reported by Kobashi [5] and the heat transfer by convection from a heated sphere rotating in air has been investigated experimentally by Nordlie and Kreith [6].

This paper corrects and extends Singh's analysis to permit theoretical calculations of the average heat-transfer coefficient for a rotating sphere, presents experimental data of convection heat-transfer coefficients to and from rotating spheres over wide ranges of Reynolds and Prandtl numbers, compares the analytical and experimental results, and presents some additional measurements of boundary-layer velocity profiles, including the extent of a turbulent separation zone which was observed in the vicinity of the equator. Motion pictures of the flow pattern were taken with the aid of a smoke type flow visualization technique and they are available on loan from the senior author.

EQUIPMENT AND EXPERIMENTAL TECHNIQUE FOR THE HEAT-TRANSFER MEASUREMENTS

The heat-transfer tests were performed with a type 2017-T-4 solid aluminum sphere, 6 inches in diameter, and with a smaller 224K aluminum–bronze sphere, 2 inches in diameter. The construction of these spheres is shown schematically in Fig. 1 and a photograph of the experimental installation is shown in Fig. 2. Each sphere was attached to a vertical hollow shaft which was driven at the top by a small motor whose rotational speed could be adjusted and controlled between 30 and 2500 r.p.m. by means of a powerstat connected to a voltage regulator. The temperature of the sphere was measured by means of a copper–constantan thermocouple which was peened near the center into the larger aluminum sphere, but immersed into a pool of mercury

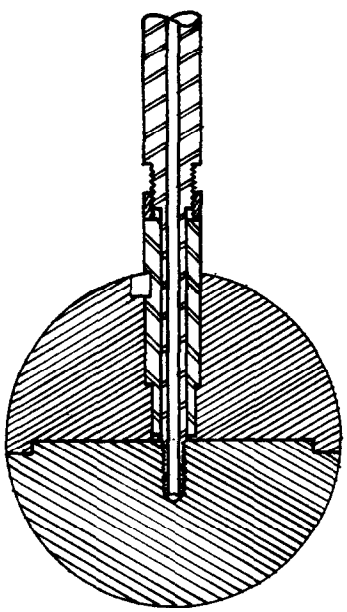

FIG. 1. Schematic sketch showing construction of the 6 in diameter aluminum sphere.

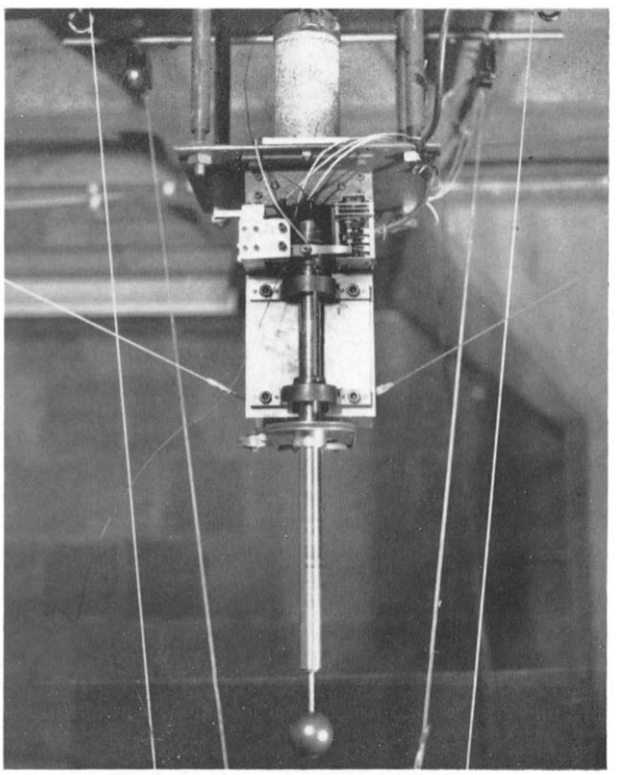

FIG. 2. Photograph of the experimental equipment used in heat-transfer tests with 2 in. diameter sphere.

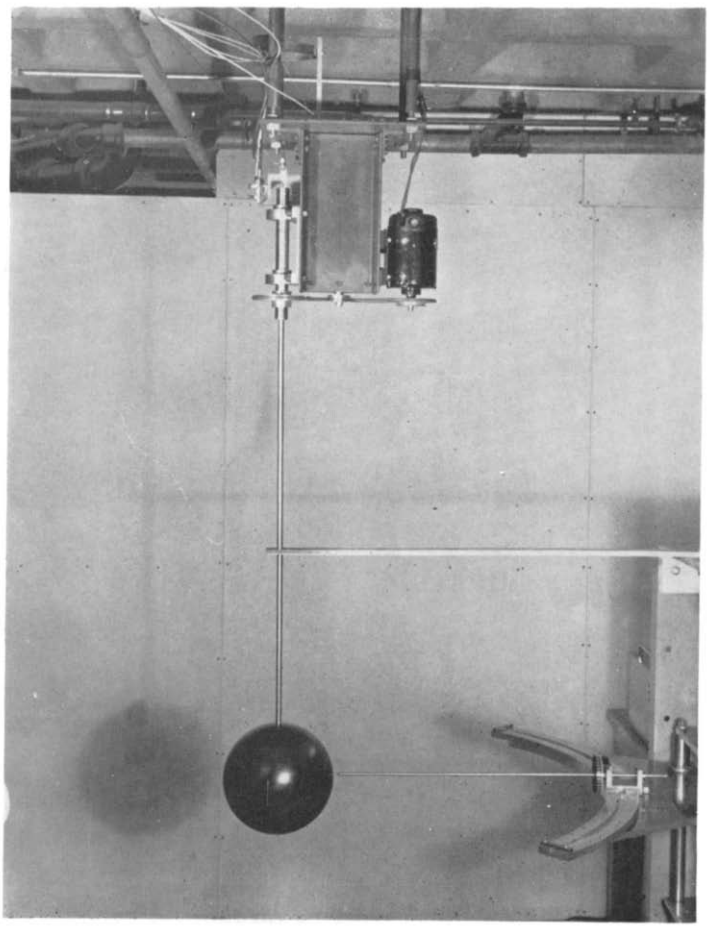

FIG. 6. Photograph of velocity magnitude and direction finder with hot wire probe and experimental equipment used in flow studies.

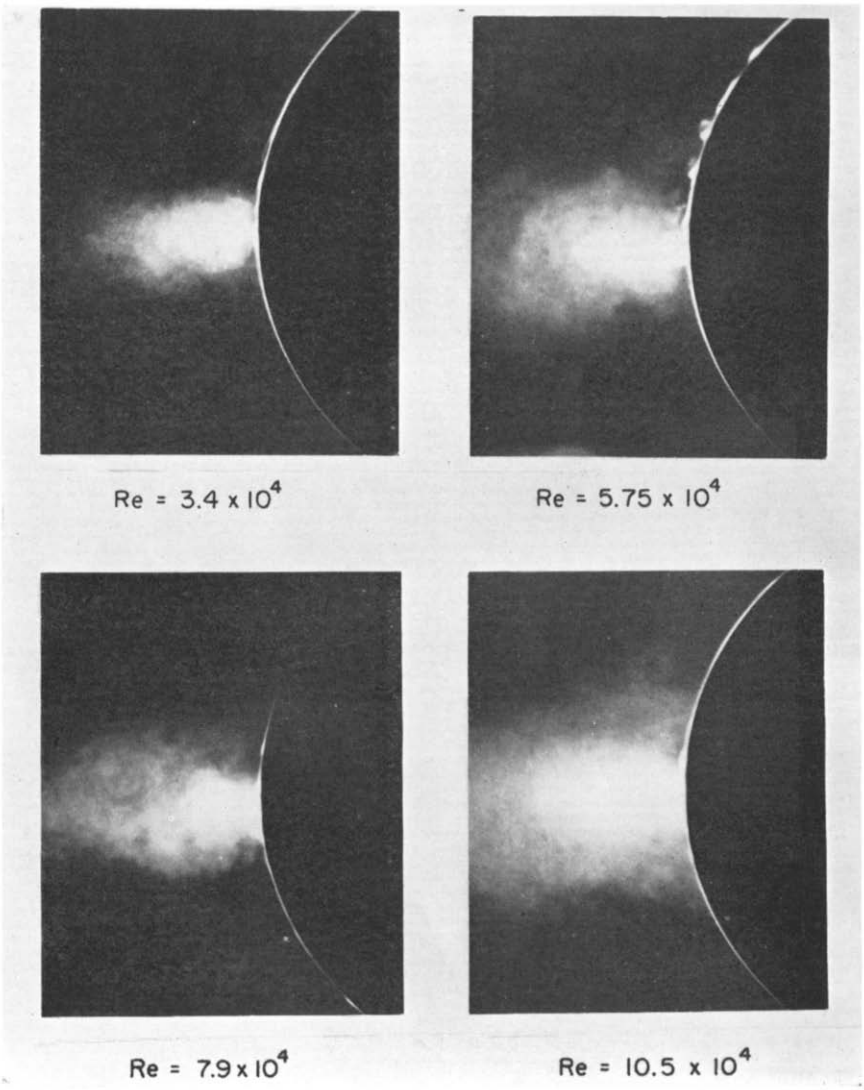

FIG. 10. Smoke photograph of the boundary-layer interaction in the vicinity of the equator at Reynolds numbers of $3{\cdot}4 \times 10^4$, $5{\cdot}25 \times 10^4$, $7{\cdot}9 \times 10^4$, and $10{\cdot}5 \times 10^4$.

inside the smaller aluminum–bronze sphere. The rotating copper lead of the thermocouple was connected to a slipring–brush arrangement equipped with an automatic timer which periodically lifted the spring-loaded brushes off the rotating slipring to prevent excessive frictional heating. Galling between the copper slip-rings and copper brushes was prevented by plating the ends of the brushes with a layer of silver which was sufficiently thin to avoid thermocouple effects. The constantan lead of the thermocouple was taken out in the center at the upper end of the shaft where the tip of a small, springloaded constantan cone which was connected to a stationary constantan wire made contact with a conical indentation in the rotating constantan wire which was attached to a nylon bushing in the shaft. In addition to the sphere temperature also the temperature of the cooling or heating medium was measured by means of a thermocouple and both temperatures were recorded as a function of time during each test on an automatic strip-chart temperature recorder.

The shaft supporting the sphere was made as small as possible to reduce heat conduction along it. Some fin action of the shaft was unavoidable, but a calculation of the maximum heat loss from the sphere along the shaft showed that it was less than 1 per cent of the total heat loss even under the most unfavorable test conditions.

The experimental technique is described in detail in [6] and [7]. Briefly, before each test the sphere was heated to about 250°F in a radiant type heating box which could be slipped over it from below. After the desired initial temperature had been reached, the motor was turned on, the speed was adjusted to the desired value, the sphere was immersed in the appropriate medium, and the temperature–time histories of the sphere and the medium were recorded on an automatic strip-chart temperature recorder. It was known from previous experiments [6] that the internal thermal resistance of a small metal sphere is so small compared to the convective thermal resistance between the surface of the sphere and its environment that the sphere may be treated as a lumped parameter system without introducing an appreciable error. The overall average heat-transfer coefficient could, therefore, be determined by means of a transient technique described in [6] and [8], which gives the equation

$$\bar{h}_c = \frac{(4/3)\,\pi a^3 \rho_s c_s\,(\mathrm{d}T_s/\mathrm{d}t)}{4\pi a^2\,(T_s - T_\infty)} = \frac{c_s \rho_s a}{3}\left[\frac{\mathrm{d}T_s(t)/\mathrm{d}t}{T_s(t) - T_\infty}\right] \qquad (1)$$

for a sphere. The slopes of the sphere temperature versus time curves, $\mathrm{d}T_s/\mathrm{d}t$, could be determined numerically from the experimental data at any time t. But in order to facilitate the reduction of the experimental data and to maintain uniformity of the physical properties in all tests, the slope of the temperature versus time curve was evaluated for each test at that instant when the arithmetic mean between the sphere temperature and the environment temperature was 100°F. A few spot checks at different temperatures showed that this procedure was satisfactory.

The average overall heat-transfer coefficient, which is the value determined by the experiments, is the sum of the average convection heat-transfer coefficient $\bar{h}_c$ and the radiation heat-transfer coefficient $\bar{h}_r$, or

$$\bar{h} = \bar{h}_c + \bar{h}_r. \qquad (2)$$

The contribution of radiative heat transfer to the total rate of heat transfer was appreciable only for tests in air. For these tests the radiation heat-transfer coefficient can be expressed in the form

$$\bar{h}_r = \epsilon\sigma(T_s^2 + T_\infty^2)\,(T_s + T_\infty) \qquad (3)$$

where T_s is the value of the sphere temperature at that time in the cooling process at which $(\mathrm{d}T_s/\mathrm{d}t)$ is evaluated. The convection heat-transfer coefficient was then obtained by subtracting the appropriate value of $\bar{h}_r$ from $\bar{h}$ according to (2). For tests with water, oil, and mercury the radiation correction is negligible.

Whereas tests in air could be made with the entire room as the environment, for tests with water, oil, and mercury, a finite container had to be used. In order to make sure that the container would be sufficiently large so that its walls would not interfere with the flow which would exist in a quasi infinite environment, a series of tests were made with the sphere rotating

first in the room and then inside the container which was later used for the tests with liquids. In no case did the heat-transfer coefficients obtained in these tests differ from each other at similar Reynolds numbers by more than 2 per cent, which is well within the accuracy of the experimental results. It may therefore be assumed that the test results for air as well as for water, oil, and mercury correspond to conditions which would obtain in an infinite medium.

EXPERIMENTAL RESULTS OF THE HEAT-TRANSFER EXPERIMENTS*

Cooling tests were performed in air, water, and oil† with the larger as well as with the smaller sphere, in mercury only with the smaller sphere, and heating tests were performed with the smaller sphere alone in water. All test results were reduced to appropriate dimensionless numbers in which the physical properties were evaluated at the arithmetic mean between the temperature of the sphere and the temperature of the surrounding medium.

Experiments with a rotating cylinder [10] and a rotating sphere [6] under conditions where both free and forced convection are significant have shown that free convection effects become negligibly small when the Grashof number is 10 per cent or less than the square of the Reynolds number. According to this criterion gravitationally induced free convection could be neglected in all tests reported here so that the Nusselt, Reynolds, and Prandtl numbers were the only variable parameters.

The experimental results are shown in Fig. 3 where the average Nusselt number $\bar{h}_c D/k_f$ is plotted as a function of the rotational Reynolds number $\Omega D_s^2/\nu_f$ for tests with both spheres in oil, water, air, and mercury. An inspection of the lines faired through the data shows that at Reynolds numbers below about 5×10^4 the Nusselt number for oil, water, and air increases with the square root of the Reynolds number. At Reynolds numbers above 5×10^5 the Nusselt number for water and air is proportional to $Re^{0.67}$, but in this range no data could be obtained with the oil because of its high viscosity.

As will be shown in more detail later on, the change in the functional relationship between $\overline{Nu}$ and Re at Re of 5×10^5 is due to a spreading

* A detailed tabulation of the data and the experimental results can be found in [7] and [9].

† The oil was Spindura BB of A.P.I, gravity 31, kindly supplied by the Texaco Company.

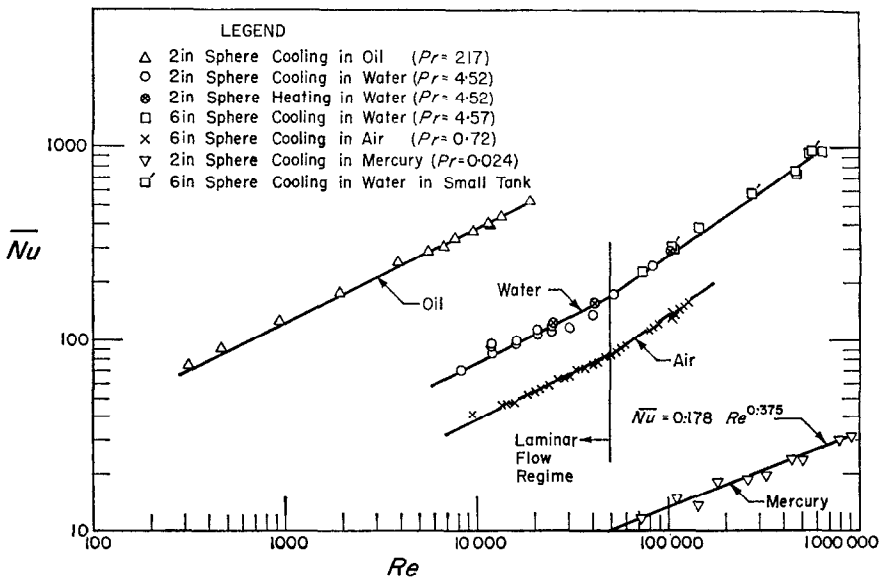

FIG. 3. Experimental results of heat-transfer tests—average Nusselt number vs. Reynolds number for air, water, oil, and mercury.

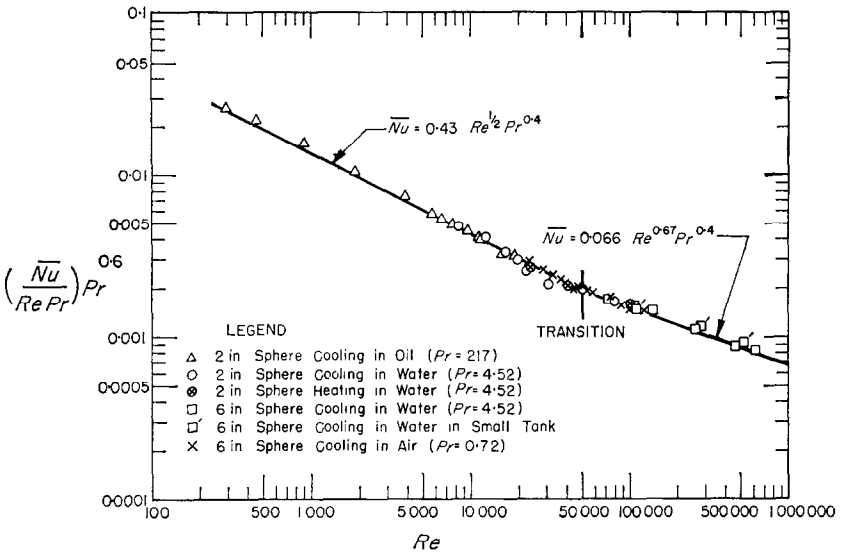

FIG. 4. Correlation of experimental results—$\overline{Nu}\ Pr^{0.4}/Re$ vs. Re.

of a turbulent separation zone in the vicinity of the equator. At Reynolds numbers below 5×10^5 the separation region was confined to less than 2° on both sides of the equator and the flow over the rest of the surface of the sphere was laminar.

In order to obtain a generalized correlation of the type $\overline{Nu} = f(Re, Pr)$ and to compare the experimental results with theoretical calculations for the average Nusselt number in the laminar flow regime (see Appendix), the Nusselt number divided by the square root of the Reynolds number was plotted as a function of the Prandtl number. Inspection of the line drawn through the experimental data showed that in the range of Prandtl numbers between 0·7 and 217, $(\overline{Nu}/Re^{1/2})$ increases with the Prandtl number raised to the 0·4 power so that a generalized correlation as shown in Fig. 4 could be obtained. Using this power dependence with the Prandtl number, which is in close agreement with forced convection correlation for other geometrical configurations [8], the following empirical relations can be obtained from Figs. 3 and 4:

$$\overline{Nu} = 0{\cdot}43\ Re^{0{\cdot}5}\ Pr^{0{\cdot}4} \quad \begin{cases} Gr < 0{\cdot}1\ Re^2 \\ Re < 5 \times 10^5 \\ 0{\cdot}7 < Pr < 217 \end{cases} \qquad (4)$$

and

$$\overline{Nu} = 0{\cdot}066\ Re^{0{\cdot}67}\ Pr^{0{\cdot}4} \quad \begin{cases} Gr < 0{\cdot}1\ Re^2 \\ 5 \times 10^5 < Re < 7 \times 10^6 \\ 0{\cdot}7 < Pr < 7. \end{cases}$$

As shown in Fig. 4, the preceding equations correlate the experimental data for convection heat transfer to or from spheres rotating in air, water, and oil within about 15 per cent over a Reynolds number range from 300 to 600 000 provided normal free convection is negligible.

The experimental results obtained when the rotating sphere was cooled in mercury did not fit the correlation obtained with fluids having Prandtl numbers the order of unity or larger. The data obtained in mercury ($Pr = 0{\cdot}024$) over a range of Reynolds numbers between 70 000 and 1 000 000 could be correlated, as shown in Fig. 3, by the empirical equation

$$\overline{Nu} = 0{\cdot}178\ Re^{0{\cdot}375}. \qquad (5)$$

It may be noted that although the Reynolds numbers fell into the partially turbulent flow regime, the Nusselt number increased only with the 0·375 power of the Reynolds number. The reason for this deviation from the trend of the data for fluids with larger Prandtl numbers is not known.

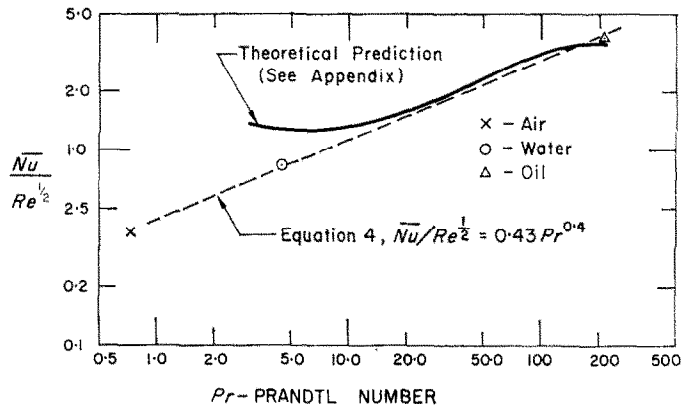

FIG. 5. Comparison of experimental and theoretical results – $\overline{Nu}/Re^{1/2}$ vs. Pr.

A comparison of the experimental results with average Nusselt numbers calculated from boundary-layer theory is shown in Fig. 5. Using a calculation procedure outlined in detail in the Appendix, the coefficients C in the equation $(\overline{Nu}/Re^{1/2}) = Cf(Pr)$ were calculated for Prandtl numbers of about 3, 6, 22, 100, and 220 and a line faired through them. As pointed out by Singh [4], the series used in the theoretical solution converges only as long as $Pr > 2$. In practice, however, the convergence was found to be very poor for Prandtl numbers less than three.

A comparison of the calculated curves with the experimental results shows that the Nusselt number predicted on the assumption of a uniform boundary-layer thickness agrees within 30 per cent with the experimental value at Prandtl numbers larger than four, but deviates considerably from the experimental results at smaller values of the Prandtl number. The discrepancy between theory and experiment is believed to be the result of neglecting the thickening of the boundary layer with increasing angular distance from the equator in the analytical solution. For a given angular increment more heat-transfer area is spanned near the equator than near the poles. Since the experimental measurements described in the following section indicate that the boundary layer thickness increases as one moves from the poles toward the equator, it appears that the assumption of a uniform boundary-layer thickness underestimates the effective thermal resistance per unit angle, measured along a big circle in the vicinity of the equator.

THE FLOW ENGENDERED BY A ROTATING SPHERE

In the analytical solution for the heat-transfer coefficient by convection to or from a rotating sphere (see Appendix), the solution of the boundary-layer flow equations constructed by Nigam [3] was used. In his solution Nigam assumed implicitly that 1. the flow is laminar over the entire surface of the sphere, 2. the thickness of the boundary layer from poles to equator is uniform over the entire sphere, and 3. the assumptions inherent in boundary layer theory do not break down at the equator.

As shown in detail by Howarth [2], the boundary-layer equations for a rotating sphere degenerate in the vicinity of the poles into the same form as the equations for a rotating disk derived by von Kármán [12]. On a rotating disk the boundary layer remains laminar at Reynolds numbers (based on the diameter) below 10^6 and since in the experiments reported here the highest Reynolds number was 9×10^5 the first assumption appeared to be reasonable except in the vicinity of the equator where, as will be discussed later in more detail, flow separation takes place and the flow becomes turbulent. The second assumption is a mere hypothesis which, although not stated by Nigam, is implied in the

series expansion used by him. The third assumption is justified by Nigam on purely formal grounds by showing that the order of magnitude assumptions leading to the boundary-layer equations do not break down at the equator. This sort of argument, however, is not realistic for a physical system in which the flow conditions on which the boundary-layer assumptions are predicated may not exist. The third as well as the second assumption can, therefore, only be verified by experiments.

The only experimental investigation of the flow engendered by a rotating sphere which has been reported heretofore was confined to a single Reynolds number. Kobashi [5] measured the velocity vector field by means of a hot wire and calculated from his measurements the tangential velocity components in the vicinity of a 0·328 ft diameter sphere rotating at 3000 r.p.m. Unfortunately [5] gives no information about the external environment; assuming that the experiments were made in air at normal temperature and pressure the experimental conditions correspond approximately to a Reynolds number of ten thousand.

For this Reynolds number the measured velocity profiles exhibited certain similarities with the velocity profiles predicted by Nigam, but the agreement was quantitatively rather poor except on one point: Nigam's theory predicts inflow into the boundary layer from the poles up to co-latitudes (measured from the pole) of 54·75° and outflow between co-latitudes of 54·75° and the equator. Kobashi's measurements indicated that a transition from inflow to outflow occurs at a co-latitude of 54·5°. Since Howarth's solution does not predict any outflow near the equator, which is of course a physical necessity without which continuity cannot be satisfied, it appeared reasonable to use Nigam's theory despite its shortcomings. In retrospect, however, the poor agreement between predicted and measured Nusselt numbers at Prandtl numbers of the order of one (see Fig. 5), raised serious doubts regarding the tenability of Nigam's assumptions as well as the reliability of Kobashi's measurements. In order to gain further insight into the convection mechanism, it was therefore deemed desirable to investigate certain key features of the flow, e.g. the distribution of the boundary-layer thickness, the extent of inflow and outflow regions, and the flow interaction at the equator.

EQUIPMENT AND EXPERIMENTAL TECHNIQUE FOR THE FLOW STUDIES

The sphere used in the experimental flow investigations was an 8·50 in diameter black ebonite bowling ball which was suspended on a $\frac{3}{8}$ in diameter shaft from supports mounted in the ceiling. The bowling ball was dynamically balanced so that vibration and wobbling were reduced to a minimum. To simulate conditions of an infinite environment the shaft was extended 30 in above the sphere because smoke visualization studies showed that this distance was sufficient to eliminate the influence of the pulleys on the flow pattern over the sphere. At its upper end the shaft was supported by precision bearings and driven by a pulley system with a small electric motor whose rotational speed could be controlled with a powerstat. The apparatus was attached to a steel frame and suspended from the ceiling as shown in Fig. 6.

The speed of rotation of the sphere was measured with a Strobotac connected in series with a Strobolux. The velocity of the flow in the boundary layer was determined on the lower half of the sphere with a Flow Corporation HWB-2 hot wire anemometer in conjunction with a velocity direction finder which was specifically designed to determine the magnitude and direction of a velocity vector in space using the co-ordinate system shown in Fig. 7.

The principal component of the velocity direction finder was a 90° arc section of 20 in radius. The end of the hot wire probe was mounted in two small bearings, so that the probe could be freely rotated about its longitudinal axis and its angular location be determined on a circular dial. The bearings were mounted on a block with two grooves which could slide on rails in the arc section. When in this arrangement the hot wire tip of the probe was placed at the center of the arc section, the tip remained stationary in space as the bearing supports were moved over the 90° interval of that section. The arc section containing the probe was mounted on a support which could be moved

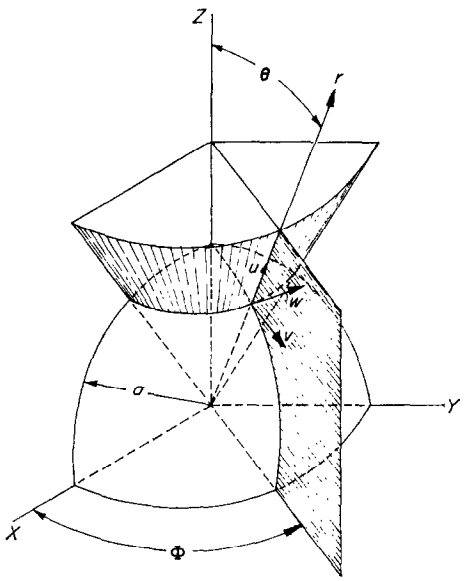

FIG. 7. Co-ordinate system for rotating sphere.

vertically and horizontally to any desired position by means of screw attachments.

To make a velocity measurement the hot wire probe was inserted into the boundary layer on the sphere at a desired position and the end at which the stem of the probe was attached to the bearings was moved horizontally to one extreme or the other on the 90° arc section. In both extreme positions, i.e. 90° apart, the hot wire probe was rotated about its longitudinal axis until the galvanometer of the hot wire system indicated a maximum unbalance, thus indicating the angular position corresponding to the maximum velocity in the plane in which the hot wire was located. Once the maximum velocity in two planes spaced 90° apart is known, it is possible to calculate the velocity vector in space since it must lie in both planes and must coincide with the line of intersection of the two planes. The magnitude and direction of the velocity could therefore be calculated from the experimentally measured values of the two velocities in the two planes of measurements. Additional details of the experimental technique, as well as the derivations of the equations necessary to calculate the direction and magnitude of a velocity vector in space are presented in [11].

EXPERIMENTAL RESULTS OF THE FLOW STUDIES

Fig. 8 shows in dimensionless form the tangential velocity component in the plane of a parallel as a function of distance from the surface of the sphere at 5°, 10° and 30° latitudes at a Reynolds number of $5{\cdot}25 \times 10^4$. To construct these figures, it was necessary to determine first the boundary-layer thickness along a meridian $\delta(\theta)$. This was done by defining the boundary layer thickness as that distance from the surface of the sphere at which the tangential velocity component in the plane of a parallel decreases to 2 per cent of the rotational speed ($a\,\Omega \sin\theta$) of the sphere surface and measuring the distance at which this condition obtained. Also shown in Fig. 8 are the tangential velocity profiles predicted by Howarth [2] and Nigam [3]. It should be noted that although two of the three measuring stations were located quite near the equator, there is remarkably close agreement between the experimental results and the velocity profile predicted by Howarth's solution which was obtained by an expansion about the pole.

Comparisons of the tangential velocity component profiles in planes of a parallel nearer the poles and the tangential velocity component in planes of a meridian did not show equally good agreement; this can be attributed mainly to limitations in the measuring equipment.

On the basis of dimensionless velocity distributions such as those shown in Fig. 8 and in [5] it is, however, not possible to evaluate the agreement between experimental measurements and the predictions made on the basis of the theories such as those by Howarth and Nigam respectively. To determine the validity of a theoretical analysis, also the actual boundary-layer thickness must be compared with that predicted from theoretical considerations. Such a comparison is shown in Fig. 9 where the variation in the experimentally measured boundary layer thickness in a meridian plane along a big circle from pole to equator is compared with the predictions of Howarth and Nigam at a Reynolds number of $5{\cdot}25 \times 10^4$. An inspection of this figure shows that the boundary-layer thickness predicted by Howarth's analysis is in good agreement with the measured values, but that Nigam's assump-

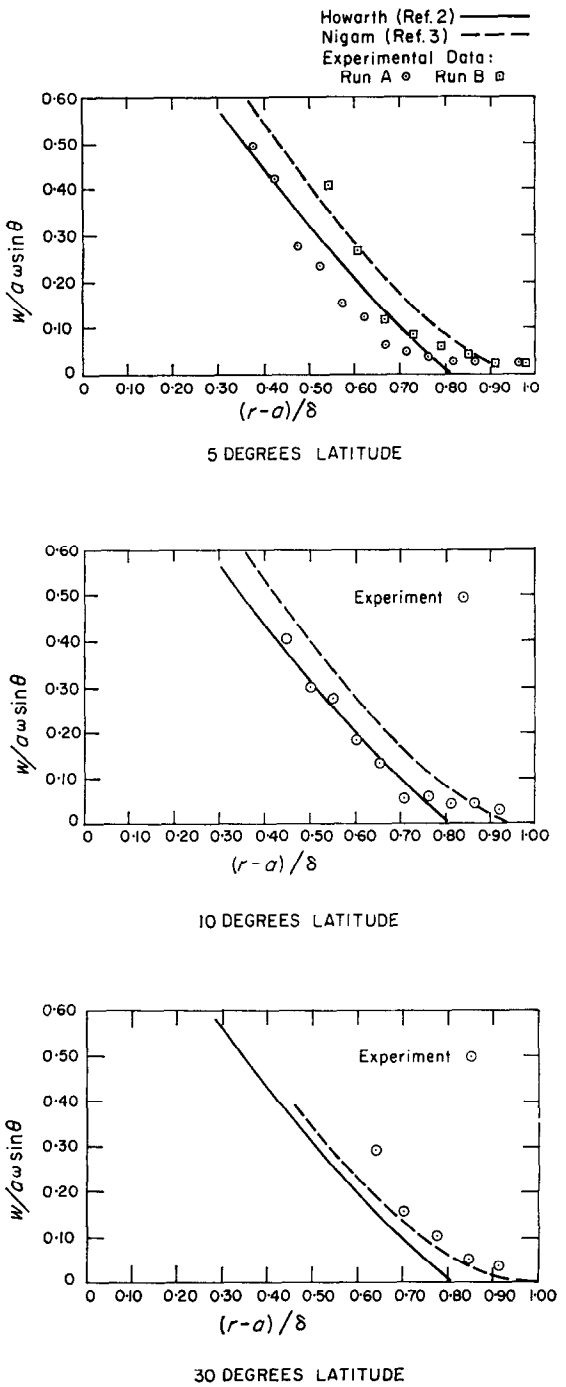

FIG. 8. Comparison of experimental and theoretical tangential velocity distribution in the plane of a parallel on a rotating sphere at a Reynolds number of $5{\cdot}25 \times 10^4$ at latitudes of 5, 10, and 30°.

tions yield much too small a boundary-layer thickness, except near the equator. This result explains at least in part why at Prandtl numbers of the order of unity the Nusselt number predicted analytically was larger than the measured values—too small a boundary-layer thickness results in too steep a velocity or temperature gradient at the surface.

The agreement between Howarth's theory and the experimentally measured boundary layer thickness raised anew the question of the extent of inflow and outflow regions, since Howarth's analysis fails to predict any outflow. Howarth attributed the cause of this failure in his solution to the limitations of the boundary-layer equations which, he said, cease to describe the flow near the equator in the region of the interaction between the two impinging layers from the upper and lower halves of the sphere.

In view of the limitations in the accuracy of the measuring equipment available to the authors, it was not possible to deduce the radial velocity component from the total velocity vector with sufficient accuracy to determine the extent of the inflow and outflow regions over the sphere with confidence. Kobashi [5], who used more refined equipment, calculated the radial component from his measurements of the total velocity vector; but in view of the extremely small order of magnitude of this velocity component, its accuracy is very questionable. Moreover, since the agreement between Nigam's prediction and Kobashi's measurements of the extent of the inflow and outflow regions had originally been a corner stone in the decision to use Nigam's solution of the boundary-layer equations in the analysis of the convection heat transfer, it was deemed desirable to investigate the radial flow pattern over the sphere in a different and more direct manner.

To obtain reliable results, the flow pattern about the sphere was studied visually in air by means of two slightly different types of flow visualization techniques. Although the techniques could not yield quantitative measures of the velocity, they did give reliable qualitative indications of the extent of the inflow and outflow regions.

In a series of tests smoke from a kerosene smoke generator was introduced into the air in

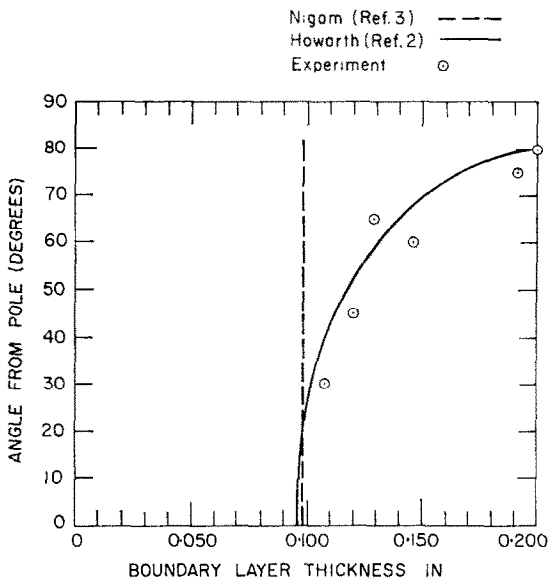

FIG. 9. Comparison of experimental and theoretical distribution of boundary-layer thickness on a sphere rotating in an infinite environment at a Reynolds number of $5{\cdot}25 \times 10^4$.

the vicinity of both poles. From there it was carried by the fan-like motion of the upper and lower halves of the sphere toward the equator, where the two streams met head on and then discharged into the room. In one series of tests the motion of the smoke was photographed in a conventional manner, with a movie camera placed some distance away from the sphere. In another series of tests pictures of the boundary layer and the separation region at the equator were obtained at various rotational speeds by placing a strong light source on one side of the sphere some distance away; the camera was then placed in such a manner that it mainly viewed light which barely grazed the sphere. Pictures obtained by this method clearly delineated the smoke filled boundary layer on the surface of the sphere, as shown in Fig. 10. It is apparent from an inspection of the photographs in Fig. 10 that at Reynolds numbers below 5×10^4 no appreciable out-flow occurred from the boundary layer over the sphere except in a very narrow zone on both sides of the equator. It is further apparent that except for the narrow separation zone at the equator the boundary layer was laminar over the entire sphere; it remained laminar over most of the sphere even when the rotational speed was increased, but increasing the Reynolds number broadened the separation zone at the equator.

The extent of separation zone about the equator was obtained quantitatively by means of the photographic methods described above and the results are shown in Fig. 11 where the width of the separation zone about the equator is plotted in degrees as a function of the Reynolds number. An inspection of this figure shows that at Reynolds numbers of about 5×10^4, the Reynolds number at which a break in the heat-transfer characteristics was observed, the separation zone begins to widen and thus introduces turbulence into the flow in the vicinity of the equator. The results of these flow studies are, therefore, in agreement with deductions from the heat-transfer results and serve to explain the overall convection characteristics of rotating spheres.

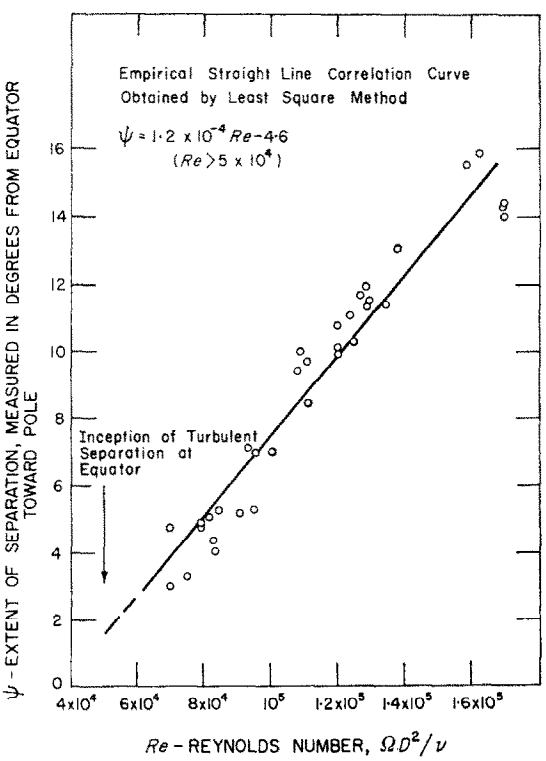

FIG. 11. Extent of turbulent separation zone in the vicinity of the equator as a function of Reynolds number.

In passing it may be of interest to note some observations regarding the mechanism by which the laminar flow underwent transition to turbulent flow. Direct visual observations, as well as movies taken of the smoke introduced into the boundary layer from both poles, showed that before transition actually occurred small turbulent spots originated in the flow. These spots broke up the laminar flow locally and closely resembled visually the formation of bubbles in a subcooled boiling liquid or the appearance of solar flares on the sun. The actual growth pattern of these turbulent spots was almost explosive in nature, but did not in all cases produce an immediate transition of the entire flow. Additional studies of the flow in the transition region would be desirable.

CONCLUSIONS

1. At Reynolds numbers below 5×10^5 the average Nusselt number for a sphere rotating in an infinite environment is given by $\overline{Nu} = 0{\cdot}43\ Re^{0{\cdot}5}\ Pr^{0{\cdot}4}$ in the range of Prandtl numbers between 0·7 and 217.

2. At Reynolds numbers between 5×10^5 and 7×10^6 the average Nusselt number for a sphere rotating in an infinite environment is given by $\overline{Nu} = 0{\cdot}066\ Re^{0{\cdot}67}\ Pr^{0{\cdot}4}$ for Prandtl numbers between 0·7 and 7.

3. At Reynolds numbers below 5×10^5 the flow induced by a sphere rotating in an infinite environment is laminar except for a small region in the vicinity of the equator where the boundary layers from the two halves of the sphere meet.

4. The turbulent interaction zone in the vicinity of the equator is less than 2° latitude in width at Reynolds numbers below 5×10^5, but increases linearly with increasing Reynolds number as shown in Figs. 10 and 11.

5. Theoretically predicted values of the Nusselt number, based on a boundary-layer model assuming a constant boundary-layer thickness, agree reasonably well with experimental measurement in the range of Prandtl numbers between 4 and 217, but deviate considerably from the experimental results at Prandtl numbers of the order of unity.

6. In the laminar flow regime the solution of the boundary-layer equations for a rotating sphere proposed by Howarth [2] predicts the velocity field closely despite its failure to predict outflow near the equator.

ACKNOWLEDGEMENT

Support of the National Science Foundation under Grant Number G-19569 is gratefully acknowledged.

REFERENCES

1. Sir G. G. Stokes, On the theories of the interna friction of fluids in motion, *Camb. Trans.* viii, 287 (1845).
2. L. Howarth, Note on the boundary layer on a rotating sphere, *Phil. Mag.*, Series 7, **42**, 1308–1315 (1951).
3. S. D. Nigam, Note on the boundary layer on a rotating sphere, *ZAMP*, **5**, 151–154 (1954).
4. S. N. Singh, Heat transfer by laminar flow from a rotating sphere, *Appl. Sci. Res.* A **9**, 197–205 (1960).
5. Y. Kobashi, Measurements of boundary layer of a rotating sphere, *J. Sci. Hiroshima Univ.* A **20**, 149–156 (1957).
6. R. Nordlie and F. Kreith, Convection heat transfer from a rotating sphere, *International Developments in Heat Transfer, Amer. Soc. Mech. Engr., New York*, 461–467 (1961).
7. L. G. Roberts, Heat transfer from a rotating sphere. Thesis, University of Colorado, Boulder, Colorado (1961).
8. F. Kreith, *Principles of Heat Transfer*, International Textbook Co., Scranton, Pa. (1959).
9. R. L. Nordlie, Heat transfer from a rotating sphere. Thesis, University of Colorado, Boulder, Colorado (1960).
10. G. S. Etemad, Free convection heat transfer from a rotating horizontal cylinder to ambient air with interferometer study of flow, *Trans. ASME*, **77**, 1287–1289 (1955).
11. J. A. Sullivan, Laminar flow about a rotating sphere in an infinite environment. Thesis, University of Colorado, Boulder, Colorado (1960).
12. Th. von Kármán, Laminare und Turbulente Reibung, *ZAMM*, **1**, 231 (1921).

APPENDIX. A THEORETICAL ANALYSIS OF THE AVERAGE NUSSELT NUMBER FOR A SPHERE ROTATING IN AN INFINITE MEDIUM.*

The flow engendered by a sphere rotating about a diameter in otherwise undisturbed fluid has been investigated by Nigam [3] who constructed solutions for this problem in the form

* The derivation of the equations for the temperature profile follow the method of [4]. They are presented here in detail because there are some heretofore uncorrected misprints in the original paper.

of power series, Subsequently, the temperature distribution in the fluid associated with the velocity field found by Nigam [3] was investigated by Singh [4] for a rotating sphere at a uniform temperature.

Assuming that there is no imposed pressure gradient or external body force, that the flow is laminar and steady, and that the derivatives with respect to ϕ vanish as a result of symmetry, the conservation equations of continuity, momentum, and energy for a sphere uniformly at a temperature T_s rotating in an infinite medium at temperature T_∞, can, subject to conventional boundary layer simplifications [2, 4], be written as

$$\frac{\partial u}{\partial r} + \frac{1}{a}\frac{\partial v}{\partial \theta} + \frac{v}{a}\cot\theta = 0 \tag{1A}$$

$$u\frac{\partial v}{\partial r} + \frac{v}{a}\frac{\partial v}{\partial \theta} - \frac{w^2\cot\theta}{a} = \nu\frac{\partial^2 v}{\partial r^2} \tag{2A}$$

$$u\frac{\partial w}{\partial r} + \frac{v}{a}\frac{\partial w}{\partial \theta} + \frac{vw\cot\theta}{a} = \nu\frac{\partial^2 w}{\partial r^2} \tag{3A}$$

and

$$c_p\left(u\frac{\partial T}{\partial r} + \frac{v}{a}\frac{\partial T}{\partial \theta}\right) = \frac{k}{\rho}\frac{\partial^2 T}{\partial r^2} + \nu\left[\left(\frac{\partial v}{\partial r}\right)^2 + \left(\frac{\partial w}{\partial r}\right)^2\right] \tag{4A}$$

where u, v, and w are the velocity components in the r, θ, and ϕ directions (Fig. 7), T is the temperature of the fluid, ρ is the density, and ν is the kinematic viscosity.

The boundary conditions are:

$$\text{at } r = a;\ T = T_s,\ u = 0,\ v = 0,\ \text{and } w = a\Omega\sin\theta \tag{5A}$$

$$\text{at } r = \infty;\ T = T_\infty,\ v = 0,\ w = 0.$$

The flow functions satisfying equations (1A)–(4A) and the boundary conditions (5A), as proposed by Nigam, are

$$\left.\begin{aligned} u &= \tfrac{1}{2}(\nu\Omega)^{1/2}(2 - 3\sin^2\theta)\\ &\quad (H_1 + \sin^2\theta H_3 + \sin^4\theta H_5 + \ldots)\\ v &= a\Omega\cos\theta(\sin\theta F_1\\ &\quad + \sin^3\theta F_3 + \sin^5\theta F_5 + \ldots)\\ \text{and}\\ w &= a\Omega\sin\theta(G_1 + \sin^2\theta G_3\\ &\quad + \sin^4\theta G_5 + \ldots). \end{aligned}\right\} \tag{6A}$$

In (6A) the F's, G's and H's are functions of $\eta = (\Omega/\nu)^{1/2}(r - a)$, and are given by

$$\left.\begin{aligned} F_1 &= C_1 s(1 + 2s)(1 - s)^2 - \frac{\delta^2}{2}s^2(1 - s)^2\\ F_3 &= C_2 s(1 + 2s)(1 - s)^2\\ F_5 &= C_4 s(1 + 2s)(1 - s)^2\\ G_1 &= \tfrac{1}{2}(2 + s)(1 - s)^2\\ G_3 &= C_3 s(1 + 2s)(1 - s)^2\\ G_5 &= C_5 s(1 + 2s)(1 - s)^2\\ -H_1 &= 4{\cdot}2822\,s^2 - 7{\cdot}271\,s^3 + 4{\cdot}5432\,s^4 - 0{\cdot}9689\,s^5\\ -H_3 &= 2{\cdot}0855\,s^2 - 3{\cdot}1283\,s^3 + 1{\cdot}6684\,s^5\\ -H_3 &= 2{\cdot}6434\,s^2 - 3{\cdot}9651\,s^4 + 2{\cdot}1147\,s^5 \end{aligned}\right\} \tag{7A}$$

where

$\eta = s\delta$, $C_1 = 1{\cdot}5183$, $C_2 = 0{\cdot}3732$, $C_3 = 0{\cdot}4257$, $C_4 = 0{\cdot}2532$, $C_5 = 0{\cdot}1949$, and $\delta = 2{\cdot}794$.

Substituting the above flow functions in the energy equation (4A), one finds [4] that the temperature distribution in the fluid is satisfied by the expression

$$c_pT = c_pT_\infty + a^2\Omega^2(M_1 + \sin^2\theta M_3 + \sin^4\theta M_5 + \ldots). \tag{8A}$$

If δ_1 is the thickness of the thermal boundary layer, the boundary conditions are:

$$\left.\begin{aligned} &M_1(0) = c_p(T_s - T_\infty)/a^2\Omega^2,\ M_3(0) = M_5(0) = 0 \text{ at } \eta = 0, \text{ on the sphere surface}\\ &\text{and } M_1(\delta_1) = 0,\ M_3(\delta_1) = 0,\ M_5(\delta_1) = 0, \text{ at the edge of the thermal boundary layer } \eta = \delta_1. \end{aligned}\right\} \tag{9A}$$

To ensure a smooth and continuous transition at the outer edge of the temperature layer it is necessary that

$$M_1'(\delta_1) = 0,\ M_3'(\delta_1) = 0,\ M_5'(\delta_1) = 0 \text{ at } \eta = \delta_1. \tag{10A}$$

The functions M_1, M_3, and M_5 satisfying the above boundary conditions are:

$$M_1 = \left[\frac{c_p(T_s - T_\infty)}{2a^2\Omega^2}\right](2 + s_1)(1 - s_1)^2 \tag{11A}$$

$$M_3 = a_1 s_1 (1 + 2s_1)(1 - s_1)^2 - \frac{0{\cdot}5835\, Pr}{2} \delta_1^2 s_1^2 (1 - s_1)^2 \quad (12A)$$

$$M_5 = b_1 s_1 (1 + 2s_1)(1 - s_1)^2 + \frac{0{\cdot}3136\, Pr}{2} \delta_1^2 s_1^2 (1 - s_1)^2 \quad (13A)$$

where $\eta = s_1 \delta_1$ and Pr is the Prandtl number.

The constants δ_1, a_1, and b_1 are determined from the following equations:

$$182{\cdot}5964\, \delta_1^3 - 70\, \delta_1^4 + 10{\cdot}7355\, \delta_1^5 - 0{\cdot}5974\, \delta_1^6 = \frac{2520}{Pr} \quad (14A)$$

$$\int_0^{\delta_1} (F_1'^2 + G_1'^2 + 3\, M_1 F_1 - 4\, M_1 F_3 - 4\, M_3 F_1)\, d\eta = \frac{M_3'(0)}{Pr} \quad (15A)$$

and

$$\int_0^{\delta_1} (F_1'^2 - 2\, F_1' F_3' - 2\, G_1' G_3' - 5\, F_1 M_3 - 5\, M_1 F_3 + 6\, F_5 M_1 + 6\, F_3 M_3 + 6\, F_1 M_5)\, d\eta = \frac{-M_5'(0)}{Pr} \quad (16A)$$

where primes denote differentiations with respect to η.

Substituting the expressions for the F's, G's and M's in equations (15A) and (16A) yields after integrating

$$d_1 + d_2 p + d_3 a_1 = 0 \quad (17A)$$

$$e_1 + e_2 p + e_3 a_1 + e_4 b_1 = 0 \quad (18A)$$

where

$$p = \frac{T_s - T_\infty}{2a^2 \Omega^2} \quad (19A)$$

and

$$\left.\begin{aligned} d_1 &= \frac{C_1^2 B}{\delta} - C_1 \delta C + \frac{\delta^3}{4} D + \frac{2}{\delta} + 1{\cdot}167\, Pr\, \delta^2 K^2 R - 0{\cdot}5835\, \delta^5 K^2 S \\ d_2 &= 3\, C_1 \delta Z - 1{\cdot}5\, \delta^3 N - 4\, C_2 \delta M \\ d_3 &= -4\, C_1 \delta P + 2\, \delta^3 Q - \frac{1}{\delta_1 Pr} \\ e_1 &= \frac{C_1^2}{\delta} B - C_1 \delta C + \frac{\delta^3}{4} D - \frac{2\, C_1 C_2}{\delta} B + 2\, C_2 \delta U + \frac{C_3}{\delta} V \\ &\quad + (1{\cdot}45875 - 1{\cdot}75050\, C_2 - 0{\cdot}9396\, C_1)\, Pr\, \delta^3 K^2 R \\ &\quad + (0{\cdot}4698\, C_1 - 0{\cdot}729375)\, Pr\, \delta^5 K^2 S \\ e_2 &= -5\, C_2 \delta M + 6\, C_4 \delta M \\ e_3 &= -5\, C_1 \delta P + \frac{5}{2} \delta^3 Q + 6\, C_2 \delta P \\ e_4 &= \frac{C_1^2 B}{\delta} - C_1 \delta C + \frac{\delta^3}{4} D + \frac{L}{\delta}. \end{aligned}\right\} \quad (20A)$$

The capital letters in the above expressions (20A) are the following polynomials in $K = (\delta_1/\delta)$

$$\left.\begin{aligned} B &= K - 6\, K^3 + 4\, K^4 + \frac{81}{5} K^5 - 24\, K^6 + \frac{64}{7} K^7 \\ C &= K^2 + 2\, K^3 - \frac{7}{2} K^4 + 14\, K^5 - 14\, K^6 + \frac{32}{7} K^7 \\ D &= \frac{4}{3} K^3 - 6\, K^4 + 10{\cdot}4\, K^5 - 8\, K^6 + \frac{16}{7} K^7 \\ L &= \frac{9}{4} K - \frac{3}{2} K^3 + \frac{9}{20} K^5 \\ M &= \frac{1}{5} K^2 - \frac{9}{70} K^4 + \frac{1}{20} K^5 \\ N &= \frac{1}{12} K^3 - \frac{3}{35} K^4 + \frac{1}{40} K^5 \\ P &= \frac{1}{15} K^2 - \frac{9}{140} K^4 + \frac{1}{36} K^5 \\ R &= \frac{1}{60} K^2 - \frac{1}{56} K^3 + \frac{1}{126} K^5 \\ S &= \frac{1}{105} K^3 - \frac{1}{84} K^4 + \frac{1}{252} K^5 \\ U &= \frac{1}{2} K^2 - K^3 + \frac{9}{4} K^4 + \frac{3}{5} K^5 - \frac{13}{3} K^6 + \frac{16}{7} K^7 \end{aligned}\right\} \quad (21A)$$

$$Y = K + \frac{10}{3}K^3 - 2K^4 - \frac{9}{5}K^5 + \frac{4}{3}K^6$$
$$Z = \frac{1}{5}K^2 - \frac{9}{70}K^4 - \frac{1}{5}K^5. \quad (21A)$$

The constant a_1 and b_1 can be evaluated from equations (17A) and (18A), or

$$a_1 = -\frac{d_1}{d_3} - \frac{d_2}{d_3}p$$
$$b_1 = -\frac{e_1}{e_4} + \frac{e_3 d_1}{e_4 d_3} + p\left(\frac{e_3 d_2}{e_4 d_3} - \frac{e_2}{e_4}\right). \quad (22A)$$

To obtain the mean value of the temperature gradient over the sphere we note that

$$c_p \frac{dT}{dr} = c_p \frac{dT}{d\eta} \cdot \frac{d\eta}{dr}$$

or

$$\frac{dT}{dr} = \frac{a^2\Omega^{5/2}}{\nu^{1/2}c_p}(M_1' + M_3' \sin^2\theta + M_5' \sin^4\theta).$$

At the surface of the sphere the mean value of the radial temperature gradient $(dT/dr)_m$ is

$$\left(\frac{dT}{dr}\right)_m = \frac{1}{4\pi a^2}\iint \frac{dT}{dr}\,dA_s = \frac{a^2\Omega^{5/2}}{\nu^{1/2}c_p} \times \left[\frac{1}{4\pi a^2}\iint (M_1' + M_3' \sin^2\theta + M_5' \sin^4\theta)\,dA_s\right] = \frac{a^2\Omega^{5/2}}{\nu^{1/2}c_p} \times \left[M_1'(0) + \frac{2}{3}M_3'(0) + \frac{8}{15}M_5'(0) + \ldots\right]. \quad (23A)$$

The average unit surface convective conductance $\bar{h}$ is defined

$$\bar{h} = -k_f (dT/dr)_{m,\text{ at surface}}/(T_s - T_\infty) \quad (24A)$$

so that the average Nusselt number can be expressed in the form

$$\overline{Nu} = 2\bar{h}\,a/k_f = -2a\,(dT/dr)_{m,\text{ at surface}}/(T_s - T_\infty). \quad (25A)$$

Combining equations (23A) and (25A) yields

$$\overline{Nu} = -\frac{2a}{T_s - T_\infty}\frac{\Omega^{5/2}a^2}{c_p\nu^{1/2}}\left[M_1'(0) + \frac{2}{3}M_3'(0) + \frac{8}{15}M_5'(0) + \ldots\right]. \quad (26A)$$

Substituting the expressions for M_1', M_3', M_5' and the constants a_1 and b_1, the preceding expression takes on the form

$$\overline{Nu} = Re^{1/2}\left[X(Pr) + Y(Pr)\frac{a^2\Omega^2}{c_p(T_s - T_\infty)}\right] \quad (27A)$$

where

$$Re = 4a^2\Omega/\nu$$
$$X(Pr) = \frac{\sqrt{(2)}}{\delta_1}\left[\frac{3}{2} + \frac{d_2}{3d_3} - \frac{4}{15}\left(\frac{e_3\,d_2}{e_4\,d_3} - \frac{e_2}{e_4}\right)\right],$$

Table 1

K	δ_1	Pr	M	N	P	Q	Z
0·8	2·2352	3·08711	0·091721	0·0157486	0·0254368	0·0052818	0·005893
0·6	1·6764	5·77	0·059226	0·008836	0·017829	0·00324	0·039786
0·35	0·9779	21·758	0·02283745	0·0024201	0·0073505	0·000962	0·02246442
0·2	0·5588	98·43	0·007811	0·000538	0·00257639	0·00022194	0·00773
0·15	0·4191	220·71	0·0044388	0·0002399	0·00146961	0·00009955	0·0044198

δ_1	e_2	e_3	e_4	d_2	d_3	$X(Pr)$
2·2352	−0·08887466	−0·092384	0·44675117	−0·8228047	−0·3461411	1·4009939
1·6764	−0·057387	−0·08995	0·345175	−0·0297782	−0·26457758	1·26628
0·9779	−0·022128	−0·057458	0·171137	0·1114606	−0·129752678	1·594112
0·5588	−0·007568	−0·026417	0·069221	0·04819458	−0·0570499	3·375
0·4191	−0·0043012	−0·01658	0·0417486	0·0298841	−0·03143597	3·561362

and

$$Y(Pr) = \frac{\sqrt{(2)}}{\delta_1}\left[\frac{2}{3}\frac{d_1}{d_3} - \frac{8}{15}\left(\frac{e_3}{e_4}\cdot\frac{a_1}{d_3} - \frac{e_1}{e_4}\right)\right].$$

For the ranges of temperatures, sphere sizes, and rotational speeds used in this investigation the quantity $a^2\Omega^2/c_p(T_s - T_\infty)$ was of the order of 10^{-3}. Since $X(Pr)$ and $Y(Pr)$ are of the same order of magnitude, the Nusselt number of equation (27A) is within an accuracy of 1 per cent given by the relation

$$\overline{Nu} = X(Pr)\, Re^{1/2}. \qquad (28A)$$

Assuming values of K, the function $X(Pr)$ was calculated for values of the Prandtl number between 3 and 220. At lower values of the Prandtl number the convergence of the series is questionable. The results of this analysis are tabulated in Table 1 and compared with the experimental data in Fig. 5.

Résumé—L'écoulement engendré par une sphère en rotation et les échanges thermiques convectifs vers ou à partir d'une telle sphère ont été étudiés expérimentalement et théoriquement pour des domaines de nombres de Reynolds allant de 0 à $9 \cdot 10^5$, des nombres de Grashof de $7 \cdot 10^4$ à $3 \cdot 10^9$ et des nombres de Prandtl de 0,024 à 217. Pour des nombres de Prandtl compris entre 4 et 217 et des nombres de Reynolds inférieurs à $5 \cdot 10^4$, le nombre de Nusselt moyen, qu'il s'agisse de chauffage ou de refroidissement, est en bon accord avec les résultats du calcul théorique fondé sur la solution des équations de la couche limite obtenue en supposant que l'épaisseur de la couche limite est constante autour de la sphère. Une étude détaillée de l'écoulement de la couche limite, au moyen d'un fil chaud et par différentes méthodes de visualisation, a montré toutefois que l'épaisseur de la couche limite croît avec la distance angulaire à partir des pôles et qu'au voisinage de l'équateur, où les couches limites des deux hémisphères de la sphère en rotation se rejoignent, il se produit un décollement très complexe. L'étendue de la région de décollement a été déterminée et on a observé quelques phénomènes de transition inhabituels.

Zusammenfassung—Die um eine rotierende Kugel entstehende Strömung und der konvektive Wärmetransport zu oder von der Kugel wurden experimentell und theoretisch im Bereich der Reynoldszahlen von 0 bis $9 \cdot 10^5$, den Grashofzahlen von $7 \cdot 10^4$ bis $3 \cdot 10^9$ und den Prandtlzahlen von 0,024 bis 217 untersucht. Für Prandtlzahlen zwischen 4,0 und 217 und Reynoldszahlen kleiner als $5 \cdot 10^4$ zeigte sich die mittlere Nusseltzahl für Kühlung wie auch für Heizung gut übereinstimmend mit dem Ergebnis einer theoretischen Analyse, die auf einer Lösung der Grenzschichtgleichungen mit konstant angenommener Grenzschichtdicke um die Kugel beruhte. Eine genauere Untersuchung der Grenzschichtströmung mit Hilfe eines Hitzdrahtes und verschiedener Methoden der Sichtbarmachung zeigte jedoch, dass die Grenzschichtdicke mit der Winkelweite von den Polen zunimmt und dass in der Äquatorgegend, wo sich die Grenzschichten der oberen und der unteren Hälfte der rotierenden Kugel treffen, eine komplexe Strömungsablösung auftritt. Die Ausdehnung des Ablösungsbereiches wurde bestimmt und einige ungewöhnliche Übergangsphänomene wurden beobachtet.

Аннотация—Экспериментально и теоретически исследовались конвективный теплообмен поверхности вращающегося шара и вызванное вращением течение среды в пределах чисел Рейнольдса от 0 до 9×10^5, Грасгофа от 7×10^9 и Прандтля от 0,024 до 217. Найдено, что для чисел Прандтля от 4,0 до 217 и чисел Рейнольдса менее 5×10^4 среднее число Нуссельта как для охлаждения, так и для нагревания хорошо согласуется с результатом теоретического анализа, основанного на решении уравнений пограничного слоя шара при условии равномерной толщины слоя. Однако, детальное исследование течения в пограничном слое с помощью метода нагретой проволоки и других способов визуализации показало, что толщина пограничного слоя в действительности возрастает с увеличением углового расстояния от полюсов. Кроме того, вблизи экватора, где смыкаются пограничные слои верхнего и нижнего полушарий, имеет место сложный отрыв потока. Определён размер области отрыва. В опытах наблюдались необычные явления перехода.